Letter

Dynamic population of multiexcitation subradiant states in incoherently excited atomic arrays

Oriol Rubies-Bigorda [1,2,*,†] Stefan Ostermann [2,*,‡] and Susanne F. Yelin [2]

[1] *Physics Department, Massachusetts Institute of Technology, Cambridge, Massachusetts 02139, USA*

[2] *Department of Physics, Harvard University, Cambridge, Massachusetts 02138, USA*

(Received 8 September 2022; revised 9 December 2022; accepted 10 April 2023; published 8 May 2023)

The deterministic generation of multiexcitation subradiant states proves to be challenging. Here, we present a viable path towards their transient generation in finite-sized ordered arrays of dipole-dipole coupled quantum emitters, based on incoherent driving of the atomic ensemble. In particular, we show that a maximal coupling to long-lived subradiant states is achieved if only half of the atoms are initially excited. We characterize the nature of the resulting states by calculating the dynamic fluorescence spectrum of the emitted light. Finally, we elucidate the role of coherent interactions during the decay process of sufficiently dense atomic arrays, which result in a coherently driven radiation burst that leads to a subsequent reduction of the chances to prepare multiexcitation subradiant states.

DOI: 10.1103/PhysRevA.107.L051701

Introduction. Recent developments in controlling and manipulating atomic ensembles in predefined geometries [1–3] open up promising avenues towards well-controlled cooperative interactions between light and matter, which are expected to be a fundamental building block for future quantum technologies [4].

If the density of the atomic ensemble is increased such that the spatial separation between atoms is smaller than or on the order of the atomic transition wavelength, light-induced dipole-dipole interactions [5,6] give rise to intriguing cooperative effects such as super- and subradiance [7–11]. State-of-the-art experiments [12–14] are now able to reach this high-density regime, which has triggered numerous studies of subradiance in ordered ensembles of quantum emitters, as well as of its applications in quantum metrology and sensing, quantum information processing, and efficient photon storage [15–26]. While most of these works focus on the single-excitation manifold where only one individual photon or excitation is shared among all atoms at a time, the preparation and analysis of subradiant states with multiple excitations has proven elusive over the years. This is due to the unfavorable scaling of the Hilbert space, as well as to the complex and nonintegrable nature of the underlying spin model, which make a thorough study of large ensembles of emitters difficult.

Here, we study this challenging multiexcitation regime and focus on the transient generation of multiexcitation subradiant states in periodic atomic arrays in free space. The combination of the Monte Carlo wave function (MCWF) method [27,28] to solve the master equation and a cumulant expansion of the Heisenberg-Langevin equations up to third order [29,30] allows us to analyze large particle numbers in the multiexcitation regime, as well as to characterize and understand the mechanisms leading to many-body subradiance. Direct addressing of individual subradiant states requires local phase

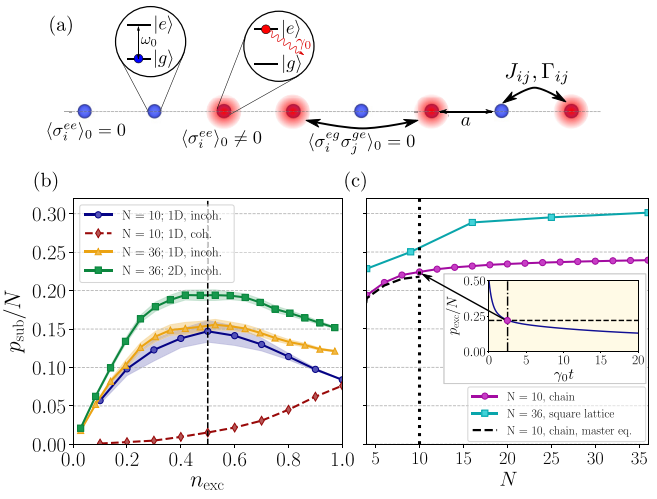

FIG. 1. (a) Sketch of a periodic chain of atoms with no pair correlations and only certain atoms excited (marked in red) at $t = 0$. (b) Magnitude of the subradiant population per particle p_{sub}/N, i.e., the excited population left in the array by the time the instantaneous decay rate $\gamma_{\mathrm{inst}} = 0.1$, as a function of excitation density n_{exc} for different array sizes and geometries. Shaded regions encompass one standard deviation. The dashed and solid lines correspond to coherent excitation and incoherent excitation, respectively. (c) p_{sub}/N as a function of atom number N for a one-dimensional chain (purple) and a two-dimensional square lattice (cyan) for an initial checkerboard excitation distribution. Third-order cumulant expansions exhibit good agreement with the master equation solutions (black dashed line). The inset shows the decay of the atomic population for a one-dimensional chain of ten atoms, as well as the time at which the system is considered to become subradiant ($\gamma_{\mathrm{inst}} = 0.1$) and p_{sub} is extracted. The lattice spacing is $a = 0.15\lambda_0$ in (b) and (c).

*O.R.-B. and S.O. contributed equally to this work.

†orubies@mit.edu

‡stefanostermann@g.harvard.edu

and amplitude imprinting via the driving field at each atomic position. While this is feasible for small numbers of qubits coupled to waveguides, where driving can occur both through the waveguide and through external sideports [25], it turns out to be elusive in free-space setups. Therefore, alternative paths towards the dynamic population of subradiant states have to be determined.

In this Letter, we outline two fundamental criteria that need to be fulfilled to dynamically populate multiexcitation subradiant states without requiring single-site addressability. First, the initially prepared state has to have a large overlap with the least radiative states of the Lindbladian spectrum [31]. We show that this can be achieved by exiting half of the atoms with no initial coherences among them, which does not require single-site addressability [32]. In this case, the system naturally evolves into a mixture of multiexcitation subradiant states. The second criterium is that the distance between atoms must be large enough such that the interaction-induced energy shifts do not lead to a population transfer from subradiant to superradiant states. If the second condition is not fulfilled, the dynamic population of bright states due to the coherent part of the atomic interactions gives rise to a rapid buildup of the atomic coherences, and the subsequent appearance of a coherently driven superradiant burst. This results in an optimal geometry or lattice spacing for which the population of multiexcitation subradiant states is maximized.

Model. We consider an ensemble of N identical two-level atoms with resonance frequency $\omega_0 = 2\pi c/\lambda_0$ that interact with the three-dimensional vacuum radiation field. Tracing out the photonic degrees of freedom under the Born-Markov approximation, one obtains the master equation for the atomic density matrix $\hat{\rho}$ [5,6,33]

$$\frac{d\hat{\rho}}{dt} = -\frac{i}{\hbar}[\hat{\mathcal{H}}, \hat{\rho}] + \mathcal{L}[\hat{\rho}], \tag{1}$$

where the Hamiltonian $\hat{\mathcal{H}}$ describes the coherent interactions between emitters

$$\hat{\mathcal{H}} = \hbar\omega_0 \sum_{n=1}^{N} \hat{\sigma}_n^{ee} + \hbar \sum_{n,m\neq n}^{N} J_{nm}\hat{\sigma}_n^{eg}\hat{\sigma}_m^{ge}, \tag{2}$$

and the Lindbladian $\mathcal{L}[\hat{\rho}]$ characterizes the dissipative interactions

$$\mathcal{L}[\hat{\rho}] = \sum_{n,m=1}^{N} \frac{\Gamma_{nm}}{2}\left(2\hat{\sigma}_n^{ge}\hat{\rho}\hat{\sigma}_m^{eg} - \hat{\sigma}_n^{eg}\hat{\sigma}_m^{ge}\hat{\rho} - \hat{\rho}\hat{\sigma}_n^{eg}\hat{\sigma}_m^{ge}\right). \tag{3}$$

Here, $\hat{\sigma}_m^{eg} = |e_m\rangle\langle g_m|$ ($\hat{\sigma}_m^{ge} = |g_m\rangle\langle e_m|$) is the raising (lowering) operator for atom m, and the coherent and dissipative parts of the dipole-dipole interactions mediated by the vacuum electromagnetic field are given by $J_{nm} - i\Gamma_{nm}/2 = -\frac{3\pi\gamma_0}{\omega_0}\mathbf{d}^\dagger\mathbf{G}(\mathbf{r}_{nm}, \omega_0)\mathbf{d}$, [5,6], where $\mathbf{d}$ is the transition dipole moment of the atoms, $\mathbf{G}(\mathbf{r}, \omega)$ is the Green's tensor for a point dipole in vacuum [32,34,35], and $\mathbf{r}_{nm} = \mathbf{r}_n - \mathbf{r}_m$ is the vector connecting atoms n and m. $\Gamma_{nn} = \gamma_0$ is the spontaneous decay rate of a single atom. The Lamb shift J_{nn} is included in the definition of the transition frequency ω_0.

Typically, the dynamics of decaying atomic ensembles are characterized by the excited-state population $p_{\mathrm{exc}}(t) = \mathrm{Tr}\{\hat{\rho}(t)\sum_n \hat{\sigma}_n^{ee}\} = \sum_n \langle\hat{\sigma}_n^{ee}\rangle(t)$ and the total photon emission rate $\gamma_{\mathrm{tot}} = -\dot{p}_{\mathrm{exc}}$. Here, we introduce the instantaneous decay rate,

$$\gamma_{\mathrm{inst}} \equiv \frac{\gamma_{\mathrm{tot}}}{p_{\mathrm{exc}}} = \gamma_0 + \frac{\sum_{n,m\neq n}\Gamma_{nm}\langle\hat{\sigma}_n^{eg}\hat{\sigma}_m^{ge}\rangle}{\sum_n\langle\hat{\sigma}_n^{ee}\rangle}, \tag{4}$$

as the figure of merit for characterizing photon emission. Unlike γ_{tot}, $\gamma_{\mathrm{inst}}(t)$ is constant for a pure exponential decay and directly reflects the superradiant ($\gamma_{\mathrm{inst}} > \gamma_0$) or subradiant ($\gamma_{\mathrm{inst}} < \gamma_0$) character of the state $\hat{\rho}(t)$ at each instant. In particular, the deviation from independent decay ($\gamma_{\mathrm{inst}} = \gamma_0$) is determined by the second term in Eq. (4) and arises from the buildup of two-body coherences $\langle\hat{\sigma}_n^{eg}\hat{\sigma}_m^{ge}\rangle$.

We employ two different numerical methods to compute the dynamics of the atomic system. For small system sizes containing up to ten atoms, we use the MCWF technique to obtain the atomic density matrix governed by the master equation (1) [27,28]. In addition, we perform a cumulant expansion of the Heisenberg-Langevin equations up to third order. To this end, we derive the equations of motion for the expectation values $\langle\dot{\hat{O}}\rangle = \mathrm{Tr}\{\dot{\hat{\rho}}\hat{O}\}$ of all operators $\hat{O}$ containing at most three atomic operators, i.e., $\langle\hat{\sigma}_i^{ee}\hat{\sigma}_j^{eg}\hat{\sigma}_k^{ge}\rangle$, and expand the averages of fourth-order operator products in terms of products of third-, second-, and first-order expectation values [29,30,32,36–38]. This approximate method allows us to study systems containing up to 36 atoms with remarkable accuracy. This is a three times larger system size than what can be simulated using the MCWF method.

Generating subradiant states. To characterize the many-body nature of the dynamically generated subradiant states, we define the subradiant population p_{sub} as the total excited-state population left in the array at the time t_{sub} at which the instantaneous decay rate reaches $\gamma_{\mathrm{inst}} = 0.1\gamma_0$. As illustrated in the inset of Fig. 1(c), this marks the point in time at which the decay of the excited-state population has drastically slowed down, indicating subradiance.

We calculate this subradiant population as a function of the excitation density $n_{\mathrm{exc}} \coloneqq N_{\mathrm{exc}}/N$, where N is the total number of atoms and N_{exc} denotes the number of initially excited emitters. First, we choose a coherent spin state of the form $|\psi_{\mathrm{coh}}\rangle = \prod_n(\sqrt{1-n_{\mathrm{exc}}}|g_n\rangle + e^{i\mathbf{k}\mathbf{r}_n}\sqrt{n_{\mathrm{exc}}}|e_n\rangle)$ as an initial state, which can be experimentally prepared by a coherent laser pulse impinging on the atomic array [20] and is typically used to study subradiance in atomic gases [23,39]. For any value of n_{exc}, the initial excited-state population is coherently shared among the atoms. While we choose $\mathbf{k} = \mathbf{0}$ for the remainder of this work, the presented results generally hold for all $\mathbf{k}$ within the light cone—defined as $|k| < 2\pi/\lambda_0$—that is, for any value of $\mathbf{k}$ that can be achieved experimentally. The red dashed line in Fig. 1(b) shows the subradiant population obtained using the MCWF approach for a chain of ten atoms prepared in $|\psi_{\mathrm{coh}}\rangle$. In this case, the subradiant population is maximal for a fully inverted system ($n_{\mathrm{exc}} = 1.0$). This phenomenon can be understood by noting that such a coherent initial state predominantly overlaps with the radiative states of the Dicke ladder [32]. Decreasing n_{exc} simply reduces the overlap with highly excited radiative states, which consequently diminishes the chance that the excitation gets trapped in subradiant states while cascading down the ladder. Note also that, for coherent initial states $|\psi_{\mathrm{coh}}\rangle$, the maximum

subradiant population is well below 10% of the total atom number. That is, once the system becomes subradiant, there is on average less than one excitation left in the system.

The value of p_{sub} can be increased if an optimized initial state is used. In particular, we find that this is the case for partially and incoherently excited arrays, i.e., for initial states of the form $|\psi_{\mathrm{incoh}}\rangle = \prod_{n\in\mathcal{E}} \hat{\sigma}_n^{eg}|G\rangle$, where $|G\rangle$ corresponds to the state where all atoms are in the ground state and $\mathcal{E}$ denotes the set of initially excited atoms. Unlike $|\psi_{\mathrm{coh}}\rangle$, $|\psi_{\mathrm{incoh}}\rangle$ has no correlations at initial times and only atomic populations are nonzero at $t = 0$ [32]. This state can thus be experimentally realized by either destroying the spatial coherence of the impinging laser via a speckle pattern or by applying a large detuning on random atoms during the coherent excitation pulse (see Supplemental Material [32]).

The solid lines in Fig. 1(b) show the subradiant population for different lattice dimensions and sizes averaged over 50 random distributions of incoherent excitations. p_{sub} is maximal if half the atoms are incoherently excited ($n_{\mathrm{exc}} = 0.5$), both for one-dimensional chains and two-dimensional square lattices, and larger values are obtained in the case of two-dimensional geometries. In any case, the fraction of atoms that remain excited for long times is on the order of 15%−20% of the total atom number, which is substantially higher than for coherently excited arrays [red dashed lines in Fig. 1(b)].

The improved behavior of the incoherent initial condition can be understood from the spectrum of the Lindbladian. As opposed to $|\psi_{\mathrm{coh}}\rangle$, $|\psi_{\mathrm{incoh}}\rangle$ has an overlap with all states within its corresponding excitation manifold, which ultimately increases the probability of dynamically populating subradiant states. The fact that the maximum p_{sub} is reached at $n_{\mathrm{exc}} = 0.5$ also makes sense intuitively, as it corresponds to the excitation manifold with the largest number of states. As a result, the overlap of the initial state with the most radiative decay channels is minimal and the probability to dynamically reach subradiant states maximal.

One can further increase the subradiant population by determining an initial state that has a larger overlap with the least radiative decay channels than the random configurations considered in Fig. 1(b). Based on intuition gained from the single-excitation manifold, where the most subradiant state is always a checkerboard pattern of positive and negative phases, we now choose initial states where only atoms located at even lattice sites are excited initially. This state can still be readily prepared without single-site addressability (see Supplemental Material for details [32]). In Fig. 1(c), we show p_{sub} as a function of atom number N. The achieved subradiant population is substantially larger than the maxima observed in Fig. 1(b), and reaches values well above 20% of the total atom number even for small systems. That is, at the time t_{sub} where the instantaneous decay rate is below $0.1\gamma_0$, a chain with ten atoms has an average of more than two excitations left. This illustrates the efficient population of two-excitation subradiant states.

Spectrum. To quantify the population that is dynamically trapped in each excitation manifold, we additionally compute the overlap $O_{N_{\mathrm{exc}}}(t) = \sum_{|\psi_i\rangle\in\Psi_{N_{\mathrm{exc}}}} \langle\psi_i|\hat{\rho}(t)|\psi_i\rangle$ of the state $\hat{\rho}(t)$ with the set of eigenstates of the Hamiltonian containing N_{exc} excitations, $\Psi_{N_{\mathrm{exc}}} = \{|\psi_1\rangle\cdots|\psi_M\rangle\}$. For an atomic array initially prepared in an incoherent checkerboard configuration, the overlap of the many-body state with manifolds containing more than one excitation ($N_{\mathrm{exc}} > 1$) is finite at long times, as shown by the black dashed-dotted curve in Fig. 2(a). This indicates that the system naturally evolves into a mixture of multiexcitation subradiant states, even for moderate array sizes of just ten atoms. As shown in Fig. 2(b) and in the Supplemental Material [32], the dynamically generated states exhibit a large overlap with the most subradiant states in each excitation manifold. This effect is particularly pronounced due to the employed checkerboard initial state, as can be seen by comparing our results to a recent work studying subradiant state generation using a statistical mixture as an initial state [39,40].

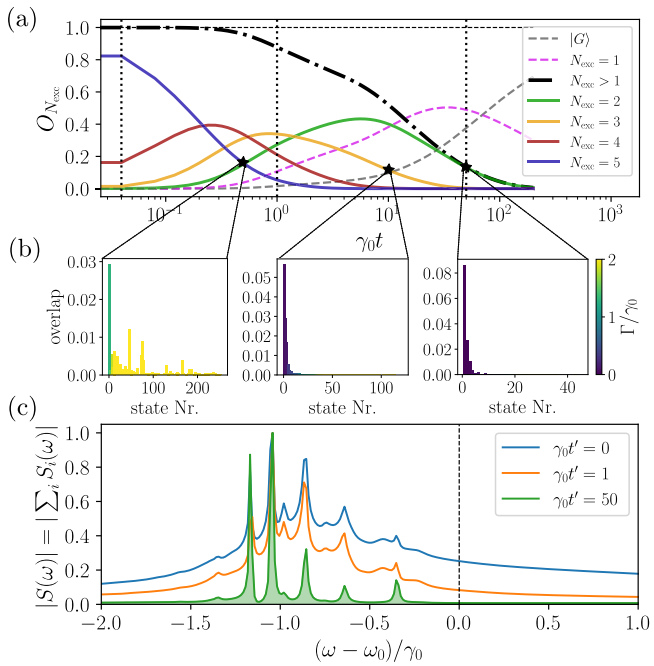

FIG. 2. (a) Overlap with the different excitation manifolds over time for a ten-atom chain ($a = 0.15\lambda_0$), with half the atoms initially excited in a checkerboard pattern. A significant contribution from multiexcitation subradiant states ($N_{\mathrm{exc}} > 1$) is observed at times $t' \gg 1/\gamma_0$. (b) Overlap of the dynamically populated state at the times indicated by black stars in (a) with each individual state contained in a given excitation manifold. Only the most subradiant states are dynamically populated. (b) Instantaneous emission spectrum at different times of the decay process. At early times (blue curve), the fast decaying superradiant states generate a broad background. The most subradiant modes persist at late times (green solid curve) and result in a discrete set of very narrow lines at fixed frequencies.

A relevant experimental observable that characterizes the subradiant nature of the state $\hat{\rho}$ is the *dynamic* fluorescence spectrum $S(\omega, t')$. If measured along the direction perpendicular to the array, the spectrum is simply given by the Fourier transform of the two-time correlation function, i.e., $S(\omega, t') = \sum_i S_n(\omega, t') = \sum_n 2\,\mathrm{Re}[\int_0^\infty d\tau e^{-i\omega\tau}\langle\sigma_n^{eg}(t'+\tau)\sigma_n^{ge}(t')\rangle]$ [41]. In Fig. 2(b), we plot the dynamic spectrum for different times t' at which the spectrum measurement begins. At early times (blue and orange curves), the fast-decaying superradiant states result in a broad background. The

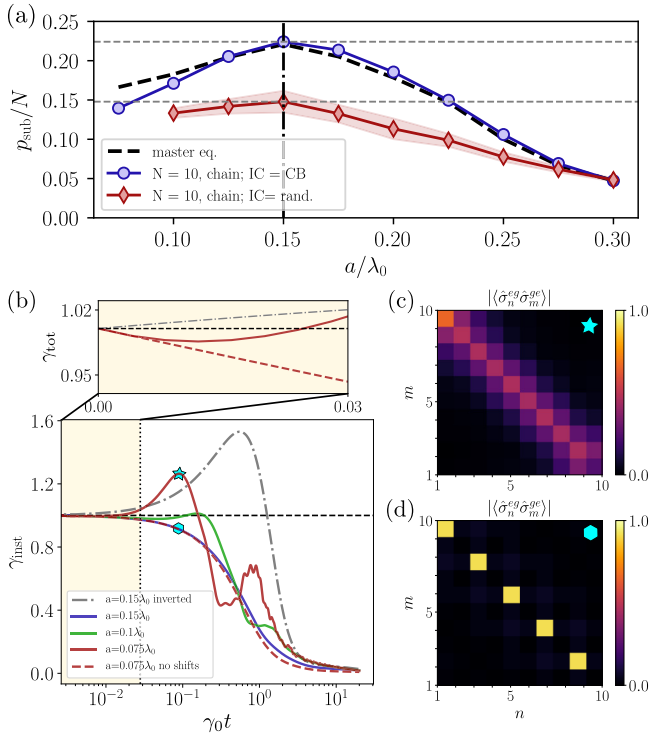

FIG. 3. (a) Subradiant population p_{sub} for an atomic chain with ten atoms as a function of lattice spacing a for a checkerboard exciation pattern (blue) and sets of five randomly excited atoms (red). The black dashed line is obtained via the master equation. (b) Normalized emission rate as a function of time for atomic chains with ten atoms and a checkerboard excitation pattern. A radiation burst emerges for small lattice spacings $a = 0.075\lambda_0$ (red curve), and disappears if coherent dipole-dipole shifts are turned off (dashed red curve). No peak appears for larger spacings ($a = 0.1\lambda_0$ in solid green and $a = 0.15\lambda_0$ in solid blue). For comparison, we also plot the superradiant peak for a fully inverted array with $a = 0.15\lambda_0$ (dashed-dotted grey curve). The upper panel shows the total photon emission rate γ_{tot} at early times. (c), (d) Populations (diagonal values) and two-body coherences $\langle\hat{\sigma}_n^{eg}\hat{\sigma}_m^{ge}\rangle$ at the time of the burst for an atomic chain with $a = 0.075\lambda_0$ (c) with ($J_{ij} \neq 0$) and (d) without ($J_{ij} = 0$) coherent shifts.

narrow peaks correspond to the long-lived subradiant states that are dynamically populated during the decay process. The late-time spectrum obtained at a finite time $t' \gg 1/\gamma_0$ does not contain any contribution from the initial superradiant decay. Hence, the broad background gets strongly suppressed and only the narrow lines remain in the spectrum. Interestingly, the frequencies of these lines do not change over time and are simply determined by the energy shifts associated to the populated subradiant eigenstates of the Hamiltonian. They can therefore be employed in cooperatively enhanced sensing protocols.

Role of coherent dynamics. Cooperative effects typically become stronger for decreasing lattice constant a. In particular, the Lindbladian in Eq. (3) approaches the Dicke limit for $a/\lambda_0 \to 0$. Intuitively, this suggests that the overlap of the initial state $|\psi_{\text{incoh}}\rangle$ with the subradiant manifold increases for decreasing a and that the subradiant population p_{sub} consequently increases, as shown in Fig. 3(a) for atomic chains with $a > 0.15\lambda_0$. If one further decreases the lattice spacing, however, the coherent dipole-dipole interactions in Eq. (2) become the largest energy scale of the system and start inducing a strong coupling between different states in the same excitation manifold. This results in a population transfer from subradiant to superradiant states, which ultimately reduces p_{sub} for small a [see Fig. 3(a)]. Thus, there is not only an optimal initial condition to dynamically populate subradiant states, but also an optimal lattice spacing or geometry.

Additionally, the appearance of large coherent interactions modifies the emission properties at early times. As shown in the top panel of Fig. 3(b), the total emission rate γ_{tot} initially decreases for states with $n_{\text{exc}} = N/2$ independent of lattice spacing. That is, the dissipative channels of the system cannot generate a fast buildup of atomic coherences to trigger the onset of a radiation burst. While this results in a monotonic decrease of the total emission at early times for $a > 0.15\lambda_0$, a radiation peak emerges for small enough lattice spacing [see the solid red curve in Fig. 3(b)]. This radiation burst originates from an excitation transfer from subradiant to superradiant states, mediated by the coherent interactions between atoms. The burst vanishes if coherent interactions ($J_{nm} = 0$) are artificially put to zero, as evinced by the dashed red curve in Fig. 3(b).

The effect can also be understood based on the two-body correlation matrix $\langle\hat{\sigma}_n^{eg}\hat{\sigma}_m^{ge}\rangle$ at the instant where the burst takes place. As shown in Figs. 3(c) and 3(d), the coherences required to observe a peak are only dynamically generated in the presence of coherent dipole-dipole interactions ($J_{nm} \neq 0$). This phenomenon is therefore different in nature from standard Dicke superradiance, where the buildup of correlations and the appearance of a radiation peak occurs due to collective dissipation, and we hereby refer to it as "coherently driven superradiance." Additionally, these findings show that the two-photon correlation function at zero time [20] can fail to capture the existence of radiation bursts for certain initial conditions of the atomic array. Finally, it is worth noting that the Hamiltonian evolution of the system can be partially engineered by adding spatial modulations of the atomic detunings, which modify the coupling between dark and bright states [21,22] and can consequently enhance or suppress the coherently driven superradiant peak [32].

Conclusions and outlook. We introduced a viable path towards the dynamic population of multiexcitation subradiant states in atomic emitter arrays that does not require local phase imprinting [25]. Our approach is based on determining an experimentally feasible initial configuration such that the dynamics results in multiexcitation subradiance. We show that incoherently exciting half of the atoms in the array and choosing a sufficiently large lattice spacing lead to a significant subradiant state population at late times. The resulting states can be characterized by means of the dynamic fluorescence spectrum, which features a peak with a narrow linewidth for each subradiant state populated at late times. These states with cooperatively reduced linewidths are a promising resource for future quantum sensing protocols involving subwavelength emitter arrays. To obtain a

good estimate of achievable sensitivities, a detailed study of realistic coherence times, the stability with respect to position fluctuations of the atoms, and the role of lattice vacancies is required [42].

We further show that a smaller atom spacing does not necessarily lead to improved multiexcitation subradiance. This occurs due to an increase of the coherent dipole-dipole interactions, which strongly couple subradiant and superradiant states and may result in a coherently driven superradiant outburst. Due to its coherent nature, this effect can be compensated and engineered by applying local ac Stark shifts to different atoms in the array [43,44]. Combining such atomic detuning patterns with tailored driving fields remains an important, mostly unexplored, avenue to prepare multiexcitation subradiant states [45,46].

Acknowledgments. We would like to thank Valentin Walther and Yidan Wang for fruitful discussions. O.R.B. acknowledges support from the CUA, as well as from Fundación Mauricio y Carlota Botton and from Fundació Bancaria "la Caixa" (LCF/BQ/AA18/11680093). S.O. is supported by a postdoctoral fellowship of the Max Planck Harvard Research Center for Quantum Optics. SFY would like to acknowledge funding from NSF through the PHY-2207972 and the QSense QLCI as well as from AFOSR.

[1] D. Barredo, S. de Léséleuc, V. Lienhard, T. Lahaye, and A. Browaeys, An atom-by-atom assembler of defect-free arbitrary two-dimensional atomic arrays, Science **354**, 1021 (2016).

[2] M. Endres, H. Bernien, A. Keesling, H. Levine, E. R. Anschuetz, A. Krajenbrink, C. Senko, V. Vuletic, M. Greiner, and M. D. Lukin, Atom-by-atom assembly of defect-free one-dimensional cold atom arrays, Science **354**, 1024 (2016).

[3] D. Barredo, V. Lienhard, S. de Léséleuc, T. Lahaye, and A. Browaeys, Synthetic three-dimensional atomic structures assembled atom by atom, Nature (London) **561**, 79 (2018).

[4] K. Hammerer, A. S. Sørensen, and E. S. Polzik, Quantum interface between light and atomic ensembles, Rev. Mod. Phys. **82**, 1041 (2010).

[5] R. H. Lehmberg, Radiation from an N-Atom System. I. General Formalism, Phys. Rev. A **2**, 883 (1970).

[6] R. H. Lehmberg, Radiation from an N-Atom System. II. Spontaneous Emission from a Pair of Atoms, Phys. Rev. A **2**, 889 (1970).

[7] R. H. Dicke, Coherence in Spontaneous Radiation Processes, Phys. Rev. **93**, 99 (1954).

[8] M. Gross and S. Haroche, Superradiance: An essay on the theory of collective spontaneous emission, Phys. Rep. **93**, 301 (1982).

[9] T. Bienaimé, N. Piovella, and R. Kaiser, Controlled Dicke Subradiance from a Large Cloud of Two-Level Systems, Phys. Rev. Lett. **108**, 123602 (2012).

[10] W. Guerin, M. O. Araújo, and R. Kaiser, Subradiance in a Large Cloud of Cold Atoms, Phys. Rev. Lett. **116**, 083601 (2016).

[11] Temporal superradiance can also occur for distant noninteracting atoms provided that the required quantum correlations are generated by conditional photon measurements [47].

[12] B. Olmos, D. Yu, Y. Singh, F. Schreck, K. Bongs, and I. Lesanovsky, Long-Range Interacting Many-Body Systems with Alkaline-Earth-Metal Atoms, Phys. Rev. Lett. **110**, 143602 (2013).

[13] J. Rui, D. Wei, A. Rubio-Abadal, S. Hollerith, J. Zeiher, D. M. Stamper-Kurn, C. Gross, and I. Bloch, A subradiant optical mirror formed by a single structured atomic layer, Nature (London) **583**, 369 (2020).

[14] S. Zhang, P. Ramchurn, K. Bongs, and Y. Singh, in *2021 Joint Conference of the European Frequency and Time Forum and IEEE International Frequency Control Symposium (EFTF/IFCS)* (IEEE, New York, 2021), pp. 1–3.

[15] G. Facchinetti, S. D. Jenkins, and J. Ruostekoski, Storing Light with Subradiant Correlations in Arrays of Atoms, Phys. Rev. Lett. **117**, 243601 (2016).

[16] A. Asenjo-Garcia, M. Moreno-Cardoner, A. Albrecht, H. J. Kimble, and D. E. Chang, Exponential Improvement in Photon Storage Fidelities Using Subradiance and "Selective Radiance" in Atomic Arrays, Phys. Rev. X **7**, 031024 (2017).

[17] M. Hebenstreit, B. Kraus, L. Ostermann, and H. Ritsch, Subradiance via Entanglement in Atoms with Several Independent Decay Channels, Phys. Rev. Lett. **118**, 143602 (2017).

[18] P.-O. Guimond, A. Grankin, D. V. Vasilyev, B. Vermersch, and P. Zoller, Subradiant Bell States in Distant Atomic Arrays, Phys. Rev. Lett. **122**, 093601 (2019).

[19] Y.-X. Zhang and K. Mølmer, Theory of Subradiant States of a One-Dimensional Two-Level Atom Chain, Phys. Rev. Lett. **122**, 203605 (2019).

[20] S. J. Masson and A. Asenjo-Garcia, Universality of Dicke superradiance in arrays of quantum emitters, Nat. Commun. **13**, 2285 (2022).

[21] O. Rubies-Bigorda, V. Walther, T. L. Patti, and S. F. Yelin, Photon control and coherent interactions via lattice dark states in atomic arrays, Phys. Rev. Res. **4**, 013110 (2022).

[22] K. E. Ballantine and J. Ruostekoski, Quantum Single-Photon Control, Storage, and Entanglement Generation with Planar Atomic Arrays, PRX Quantum **2**, 040362 (2021).

[23] G. Ferioli, A. Glicenstein, L. Henriet, I. Ferrier-Barbut, and A. Browaeys, Storage and Release of Subradiant Excitations in a Dense Atomic Cloud, Phys. Rev. X **11**, 021031 (2021).

[24] A. Piñeiro Orioli, J. K. Thompson, and A. M. Rey, Emergent Dark States from Superradiant Dynamics in Multilevel Atoms in a Cavity, Phys. Rev. X **12**, 011054 (2022).

[25] M. Zanner, T. Orell, C. M. F. Schneider, R. Albert, S. Oleschko, M. L. Juan, M. Silveri, and G. Kirchmair, Coherent control of a multi-qubit dark state in waveguide quantum electrodynamics, Nat. Phys. **18**, 538 (2022).

[26] M. Reitz, C. Sommer, and C. Genes, Cooperative Quantum Phenomena in Light-Matter Platforms, PRX Quantum **3**, 010201 (2022).

[27] R. Dum, P. Zoller, and H. Ritsch, Monte Carlo simulation of the atomic master equation for spontaneous emission, Phys. Rev. A **45**, 4879 (1992).

[28] K. Mølmer, Y. Castin, and J. Dalibard, Monte Carlo wavefunction method in quantum optics, J. Opt. Soc. Am. B **10**, 524 (1993).

[29] R. Kubo, Generalized Cumulant Expansion Method, J. Phys. Soc. Jpn. **17**, 1100 (1962).

[30] D. Plankensteiner, C. Hotter, and H. Ritsch, QuantumCumulants.jl: A Julia framework for generalized mean-field equations in open quantum systems, Quantum **6**, 617 (2022).

[31] This overlap is clearly always maximal for individual subradiant states contained in the spectrum. However, addressing these states is elusive in free-space platforms, where incoming fields only predominantly couple to the superradiant modes of the atomic ensemble.

[32] See Supplemental Material at http://link.aps.org/supplemental/10.1103/PhysRevA.107.L051701 for the definition of the Green's tensor, details on the employed third-order cumulant expansion, additional data on state overlaps with excitation manifolds, state preparation schemes, and the role of additional detuning patterns.

[33] C. Cohen-Tannoudji, J. Dupont-Roc, and G. Grynberg, *Atom-Photon Interactions: Basic Process and Applications* (John Wiley & Sons, New York, 1998).

[34] W. C. Chew, *Waves and Fields in Inhomogeneous Media* (John Wiley & Sons, New York, 1999).

[35] L. Novotny and B. Hecht, *Principles of Nano-Optics* (Cambridge University Press, Cambridge, UK, 2006).

[36] S. Krämer and H. Ritsch, Generalized mean-field approach to simulate the dynamics of large open spin ensembles with long range interactions, Eur. Phys. J. D **69**, 282 (2015).

[37] F. Robicheaux and D. A. Suresh, Beyond lowest order mean-field theory for light interacting with atom arrays, Phys. Rev. A **104**, 023702 (2021).

[38] O. Rubies-Bigorda, S. Ostermann, and S. F. Yelin, Characterizing superradiant dynamics in atomic arrays via a cumulant expansion approach, Phys. Rev. Res. **5**, 013091 (2023).

[39] A. Cipris, N. A. Moreira, T. S. do Espirito Santo, P. Weiss, C. J. Villas-Boas, R. Kaiser, W. Guerin, and R. Bachelard, Subradiance with Saturated Atoms: Population Enhancement of the Long-Lived States, Phys. Rev. Lett. **126**, 103604 (2021).

[40] A. C. Santos, A. Cidrim, C. J. Villas-Boas, R. Kaiser, and R. Bachelard, Generating long-lived entangled states with free-space collective spontaneous emission, Phys. Rev. A **105**, 053715 (2022).

[41] R. J. Glauber, Coherent and Incoherent States of the Radiation Field, Phys. Rev. **131**, 2766 (1963).

[42] C. L. Degen, F. Reinhard, and P. Cappellaro, Quantum sensing, Rev. Mod. Phys. **89**, 035002 (2017).

[43] T. Chalopin, Optical superlattices in quantum gas microscopy, Nat. Rev. Phys. **3**, 605 (2021).

[44] M.-D. Li, W. Lin, A. Luo, W.-Y. Zhang, H. Sun, B. Xiao, Y.-G. Zheng, Z.-S. Yuan, and J.-W. Pan, High-powered optical superlattice with robust phase stability for quantum gas microscopy, Opt. Express **29**, 13876 (2021).

[45] K. Stannigel, P. Rabl, and P. Zoller, Driven-dissipative preparation of entangled states in cascaded quantum-optical networks, New J. Phys. **14**, 063014 (2012).

[46] A. N. Poddubny, Driven anti-Bragg subradiant correlations in waveguide quantum electrodynamics, Phys. Rev. A **106**, L031702 (2022).

[47] M. Bojer and J. von Zanthier, Superradiance of non-interacting atoms, arXiv:2206.14646.